Self-Assembly of All-DNA Rods with Controlled Patchiness

Katarina Gvozden, Sanja Novak Ratajczak, Alberto G. Orellana, Emmanuel Kentzinger, Ulrich Rücker, Jan K. G. Dhont, Cristiano De Michele,* and Emmanuel Stiakakis*

Double-stranded DNA (dsDNA) fragments exhibit noncovalent attractive interactions between their tips. It is still unclear how DNA liquid crystal self-assembly is affected by such blunt-end attractions. It is demonstrated that stiff dsDNA fragments with moderate aspect ratio can specifically self-assemble in concentrated aqueous solutions into different types of smectic mesophases on the basis of selectively screening of blunt-end DNA stacking interactions. To this end, this type of attractions are engineered at the molecular level by constructing DNA duplexes where the attractions between one or both ends are screened by short hairpin caps. All-DNA bilayer and monolayer smectic-A type of phases, as well as a columnar phase, can be stabilized by controlling attractions strength. The results imply that the so far elusive smectic-A in DNA rod-like liquid crystals is a thermodynamically stable phase. The existence of the bilayer smectic phase is confirmed by Monte-Carlo simulations of hard cylinders decorated with one attractive terminal site. This work demonstrates that DNA blunt-ends behave as well-defined monovalent attractive patches whose strength and position can be potentially precisely tuned, highlighting unique opportunities concerning the stabilization of nonconventional DNA-based lyotropic liquid crystal phases assembled by all-DNA patchy particles with arbitrary geometry and composition.

1. Introduction

Blunt-end stacking interactions are weak attractions between the ends of two double-stranded DNA (dsDNA) helices that each

terminate in a base-pair (bp). These blunt-end attractions originate from a combination of several non-covalent interactions.[1] Together with the Watson–Crick base pairing[2] the blunt-end interactions are the most important contributions into the overall DNA double helix thermodynamic stability. These noncovalent base-stacking interactions are by now well-known to play a key role in DNA replication.[3] In addition, self-assembly studies on concentrated aqueous solutions of blunt-ended short B-form dsDNA and RNA helices have raised the hypothesis that these stacking forces could have influenced molecular evolution in prebiotic environments.[4,5] More recently, in a nonbiological context, these stacking forces were exploited to create specific molecular recognition, suggesting a parallel to base-pairing mode of assembly in the field of DNA nanotechnology.[6,7] Furthermore, in the research area of DNA lyotropic liquid crystals (LLC),[4,8–14] the base-stacking and in particular the blunt-end stacking interaction, was hypothesized to be an essential ingredient that governs the unusual bulk phase behavior[4] in moderately concentrated aqueous-saline solutions of short dsDNA fragments with a length L corresponding to N_{bp} values between 6–20 bp (with N_{bp} the number of bp) and geometrical diameter $D = 2$ nm. With the relatively large persistence length of dsDNA, $l_p^{dsDNA} \approx 50$ nm ≈ 150 bp, the above rod-like blunt-ended dsDNA fragments with aspect ratios in the range of $1 < L/D < 3.5$, are found to exhibit various LLC phases above a critical concentration, including chiral nematic (cholesteric) and columnar. This unexpected finding, which violates the molecular shape anisotropy criterion that molecular theories[15,16] and simulations[17–20] demand for a purely entropy-driven phase transition from an isotropic (I, randomly oriented) fluid phase to a nematic (N, orientationally ordered around a director) phase, was attributed to the noncovalent end-to-end aggregation of these blunt-ended DNA helices.[4] This results in the formation of polydisperse rod-like aggregates which possess a sufficiently large aspect ratio to form a cholesteric (chiral nematic, N^*) LLC phase. In addition, the same stacking attraction was suggested as a key mechanism in the formation and stability of a novel smectic LLC phase in concentrated aqueous suspensions of blunt-ended all-DNA chain-stick constructs (gapped DNA duplexes), with the molecules attaining a folded conformation in this layered mesophase.[13,21]

The question arises whether, due to the blunt-end stacking interactions, linear DNA duplexes could be viewed as an

K. Gvozden, S. Novak Ratajczak, J. K. G. Dhont, E. Stiakakis
Biomacromolecular Systems and Processes
Institute of Biological Information Processing (IBI-4)
Forschungszentrum Jülich, D-52425 Jülich, Germany
E-mail: e.stiakakis@fz-juelich.de

A. G. Orellana, C. De Michele
Dipartimento di Fisica
Sapienza Universita di Roma
Piazzale A. Moro 5, Roma 00185, Italy
E-mail: cristiano.demichele@roma1.infn.it

E. Kentzinger, U. Rücker
Jülich Centre for Neutron Science JCNS and Peter Grünberg Institut PGI
JARA-FIT
Forschungszentrum Jülich, D-52425 Jülich, Germany

anisotropic patchy rod-like particle, where the patchiness can be engineered through selective blunting suppression. In the present study we investigate the role played by blunt-end patchy attractions on the liquid crystalline phase behavior of monodisperse short and stiff dsDNA fragments, with an aspect ratio $L/D \approx 8.1$ and $L/l_p \approx 0.32$. We selectively screen blunt-end attractions of one or both of the blunt ends with short hairpin caps or a short nonsticky single-stranded DNA (ssDNA) dangling chain (as depicted in **Figure 1**A). Rod-like particles with purely repulsive interactions and such a degree of anisotropy are expected to form various LLC phases at sufficient high densities,[18–20,22–24] including a smectic phase, wherein the molecules have nematic orientational order and in addition they are organized in layers perpendicular to the nematic director. It is particular important to emphasize that the absence of a smectic phase in DNA rod-like liquid crystals still remains not fully understood.
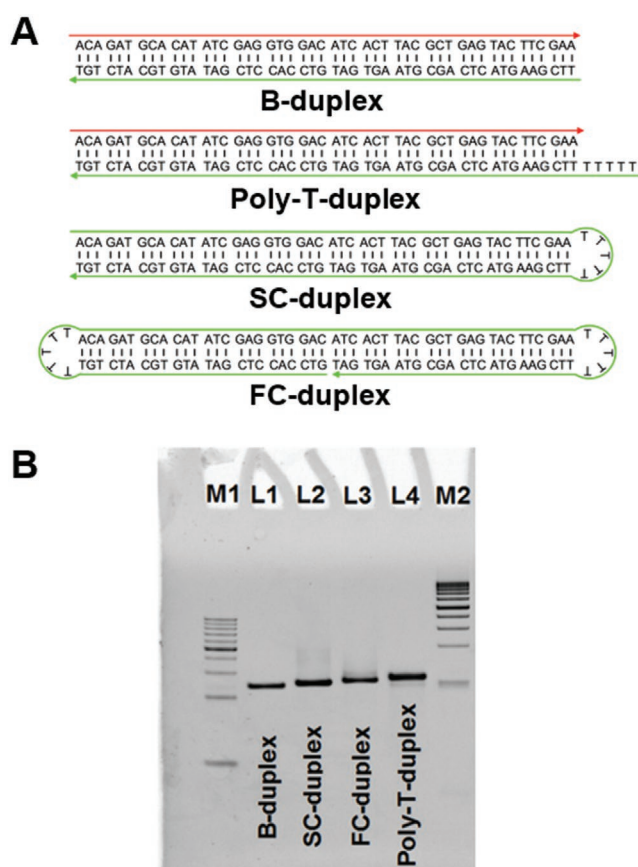

Figure 1. Design and characterization of DNA duplexes with various terminal modifications. A) Schematic drawings of the DNA duplexes employed for the exploration of the LLC behavior of rod-shaped molecules with tunable end-to-end stacking interactions. The dsDNA fragments have duplex length of 48 bp. From the top to the bottom: Blunt-ended DNA duplex which is referred to as "B-duplex," DNA duplex with 5 thymine (T) bases long nonsticky end "Poly-T-duplex", DNA duplex semi-capped by 5T loop at one end "SC-duplex", and DNA duplex full-capped by 5T loop at both ends "FC-duplex", B) Nondenaturating 10% polyacrylamide gel electrophoresis (PAGE) image. Lanes M1 and M2 contain 20 and 50 bp DNA marker, respectively. Lanes L1 to L4 correspond to B-duplex, SC-duplex, FC-duplex, and Poly-T-duplex, respectively.

We herein demonstrate that stiff dsDNA fragments can self-assemble into different types of 1D layered smectic phases in aqueous solutions on the basis of hairpin-capped DNA blunt-ends. A combination of small-angle X-ray scattering (SAXS) and computer simulations reveal that DNA helices capped on one or both ends with short poly-thymine (poly-T) loops can form thermodynamically stable bilayer and monolayer smectic-A type of phases, respectively. Our results offer insight concerning the role of blunt-end stacking interactions in DNA self assembly, allowing to identify general guidelines for the re-examination of the liquid crystalline phase diagram of short duplex DNA fragments with any length $L < l_p^{dsDNA}$.

2. Results

2.1. Synthesis

Figure 1A shows the schematic drawings and DNA sequences of the blunt-ended DNA duplex (the first cartoon from the top) and its terminal modifications. Two design principles were used for inhibiting the intermolecular base-stacking interaction between blunt-ended DNA helices.[4,25,26] The first design is based on the formation of a helix with one non-sticky ssDNA dangling tail, 5T-base-long (the second cartoon from the top in Figure 1A). In the second design, hairpin-inspired structures are formed, where a long ssDNA self-folds through intramolecular base pairing to a duplex with one or both ends capped by an unpaired, single-stranded loop, 5T-base-long (the last two cartoons from the top in Figure 1A).

The systems involved in this study are strictly monodisperse all-DNA linear structures with a fixed length of the stiff dsDNA part, $L_{dsDNA} = 48\,bp \approx 16.3\,nm$ (using 0.34 nm per bp) that is smaller than the dsDNA persistence length $l_p^{dsDNA} \approx 50\,nm$. The flexible ssDNA parts (tail and loop) consist of a poly-T sequence due to its significantly reduced tendency to form secondary structures. The poly-T sequence is chosen over poly-adenine (poly-A) due to the fact that base-stacking is weakest (or almost absent) among thymines (T) and strongest among adenines (A). Therefore, poly-T is expected be closer in a random-coil form.[27] Concerning the length of the hairpin cup, it is known that, four-base loop is close to the minimum sterically acceptable length;[28] with the best studied of the loop sequences to be 4T.[29] In our work, a 5T base-long hairpin cap is chosen as a fair compromise for a stable folding without altering the rod-like character of our DNA duplexes. The unmodified and tail-modified blunt-ended DNA duplexes were obtained by the self-assembly of two complementary synthetic ssDNA strands in 1:1 stoichiometric ratio (red and green ssDNA sequences in Figure 1A). The semi- or full-capped DNA duplexes with poly-T loops are formed by the self-assembly of one long synthetic ssDNA sequence (red ssDNA sequences in Figure 1A). The above all-DNA duplexes were synthesized through a standard thermal annealing protocol[13] (for further details see Experimental Section). We will refer to these four DNA duplexes as the B-duplex, Poly-T-duplex, SC-duplex, and FC-duplex, respectively. Polyacrylamide gel electrophoresis (PAGE) was employed to confirm the successful assembly of these duplexes. As shown in Figure 1B, the desired all-DNA constructs migrate as single

sharp bands; with the SC-duplex, FC-duplex, and Poly-T-duplex showing decreasing mobility compared to B-duplex, owing to the presence of the protruding non-sticky end and loop features.

The concentration-dependent self-assembly behavior of the proposed DNA duplexes in aqueous saline solutions was studied employing synchrotron and in-house small angle X-ray scattering (SAXS) and polarized optical microscopy (POM) measurements. All experiments reported here were performed at room temperature. Computer simulations were carried out to assess the emergence and thermodynamic stability of layered mesophases and are discussed in the Section 2.4 below.

2.2. Impacts of Blunt-End Stacking Suppression on DNA LLC Ordering

Aqueous saline solutions of concentrated B-duplexes are found to form LLC phases similar to those observed for dsDNA fragments with contour length of the order of the persistence length.[12,13] With increasing B-duplex concentration, a two-phase coexistence appears at the transition from I to LLC, and the solution becomes fully LLC at a DNA concentration of 200 mg mL^{-1}. This transition is clearly demonstrated in the POM images of the samples presented in the top inset of **Figure 2**A. Combination of SAXS measurements and observations using POM have confirmed the existence of N^* and Col phases. However, there is no evidence that smectic ordering does occur.

1D-SAXS data at room temperature for the B-duplex are shown Figure 2A for concentrations below and well above the two-phase coexistence region. These scattered intensity profiles are produced by radially averaging the recorded 2D-scattering patterns, an example of which is shown in Figure 2C. The SAXS profiles of the B-duplex for DNA concentrations around the biphasic region (see Figure 2A, second panel from the bottom, 184.5 mg mL^{-1}) are characterized by a single, broad peak, with the maximum of the scattered intensity located at scattering wave vector value q_{DNA} above $q > 1\,\mathrm{nm}^{-1}$. The first three bottom panels in Figure 2A show that a concentration increase from the nonbirefringent I (184.5 mg mL^{-1}) to one-phase birefringent phase (192.7 mg mL^{-1}) shifts the q_{DNA} to higher q-values, accompanied by a narrowing of the peak width. The broad character of this peak and the corresponding spatial correlation values ($2\pi/q_{DNA}$) indicate the presence of a liquid-like translational order between neighboring, parallel DNA helices. In addition, the POM image (Figure S1A, Supporting Information), taken within the LLC phase, close to I/LLC coexistence, displays a typical fingerprint texture characteristic for N^* phase with cholesteric pitch of the order of 2 μm.

Above the I/N^* transition, the value of q_{DNA} seems to moves slowly toward higher q-values with increasing DNA concentration as expected, verifying the structural origin of this peak. However, the 1D-SAXS pattern at DNA concentration of 275.3 mg mL^{-1} (fourth panel from the bottom in Figure 2A) is characterized by a single narrow X-ray Bragg reflection of high intensity, superimposed on the broad peak. Further increasing the B-duplex concentration (297.2 mg mL^{-1}) results in significant weakening of the broad peak, and only the sharp q_{DNA} peak remains with the wave vector corresponding to the intensity maximum shifts to higher values. The intense and sharp

features of the q_{DNA} peak reflect strong lateral positional order between B-duplex molecules and is related to the appearance of a hexagonal-columnar DNA mesophase.[9] Finally, the coexistence of a broad and a sharp q_{DNA} peak indicates a discontinuous transition from the N^* to Col phase, in agreement with previous SAXS studies on concentrated aqueous solutions of narrow polydispersity dsDNA fragments with a contour length near the persistence length.[30] The main reasons for the absence of a smectic phase in a system of rod-like particles with sufficient shape anisotropy can be rooted to particle flexibility and/or length polydispersity. Since, B-duplexes are strictly monodisperse with significant stiffness ($L/l_p \approx 0.32$) and anisotropy ($L/D > 8$), the only reason left standing to explain the absence of such a layered LLC phase is the presence of an "effective" length polydispersity resulting from the monovalent attractive interactions between their terminal base pairs.

Previous studies on ultrashort DNA duplexes have demonstrated that unpaired, ssDNA dangling tails can disturb the above type of terminal adhesion.[4] In order to asses the screening efficiency of the poly-T overhangs, the B-duplex is modified on one side with a 5T-tail (the poly-T-duplex in Figure 1A). In addition, screening of one or both attractive blunt-ends is achieved by a 5T-loop (the SC-duplex and FC-duplex in Figure 1A, respectively). If the above DNA duplex terminal modifications can efficiently screen the base-stacking forces, only monomers and dimers can be formed for the FC-duplex and SC-duplex, Poly-T-duplex respectively.

A combination of SAXS and POM measurements for these systems at different DNA concentrations is presented in Figure 2. For the Poly-T-duplex (Figure 2B), the concentration-dependent LLC phase sequence is found to be similar to the B-duplex. Starting from concentrations well above the I/LLC transition, the 1D-SAXS profile (Figure 2B, first panel from the top, 371.0 mg mL^{-1}) obtained from the 2D-SAXS pattern of Figure 2D reveal the formation of a Col phase. Further decrease of the DNA concentration results to significant broadening of the q_{DNA} peak (Figure 2B, second panel from the bottom, 250.5 mg mL^{-1}), which can be assigned to the formation of a N^* mesophase. This type of LLC phase it is attested by the cholesteric stripe texture of the sample under cross-polarizers (Figure S1B, Supporting Information). Similar to the case of B-duplex, a coexistence of the Col and N^* phase is also evidenced by the shape of the q_{DNA} peak in the 1D-SAXS profile for 339.4 mg mL^{-1} (Figure 2B, second panel from the top).

Strikingly different, however, is the phase behavior of the SC-duplex (Figure 2E) for concentrations in the range 300.2–366.1 mg mL^{-1}. In this concentration region, which is located between Col (Figure 2E, first panel from the top, 380.9 mg mL^{-1}) and N^* (Figure 2E, second panel from the bottom, 290.3 mg mL^{-1} and POM image in Figure S1C, Supporting Information), the 1D-SAXS profiles (Figure 2E, second and third panel from the top, $q < 1.0\,\mathrm{nm}^{-1}$) exhibit smectic peaks following the ratio $q/q^* = 1: 2: 3: 4$. The position of the first and most intense diffraction peak q^* corresponds to a lamellar structure with a distance between neighboring layers of $d = 2\pi/q^* = 35.6\,\mathrm{nm}$. The observed layer spacing nicely matches the length of two molecules and implies a bilayer-like packing scenario within the smectic layers, in which the SC-duplexes are arranged in coaxial stacking manner through the
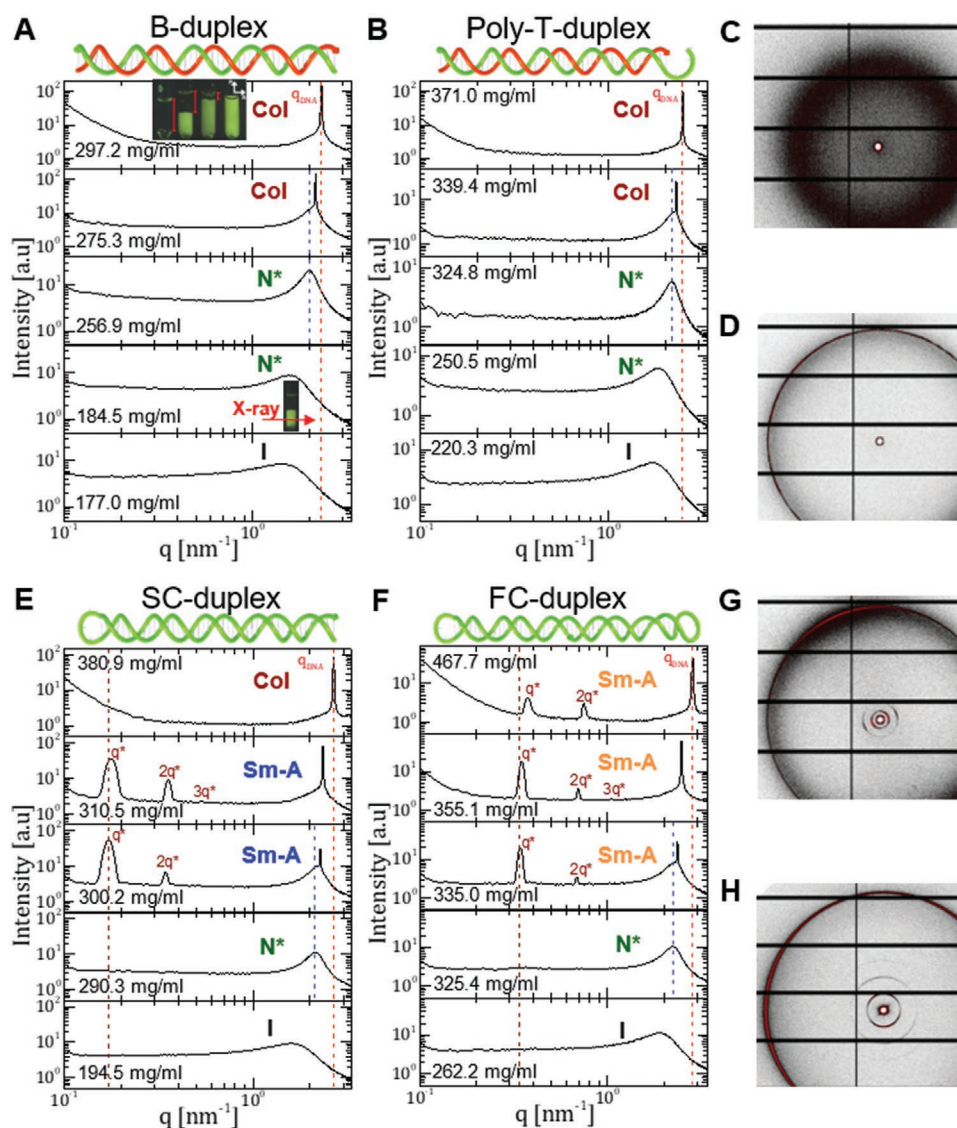
ADVANCED
SCIENCE NEWS
www.advancedsciencenews.com

NANO · MICRO
small
www.small-journal.com

Figure 2. Self-assembly of B-duplex, poly-T-duplex, SC-duplex, and FC-duplex. A) 1D-SAXS profiles for the B-duplex at various concentrations. The sample with total DNA concentration of $184.5\,\mathrm{mg\,mL^{-1}}$ exhibits a two-phase coexistence. The inset in the top-panel shows B-duplex samples observed between crossed polarizers (total DNA concentrations from left to right: 177.0, 184.5, 192.7, and $205.1\,\mathrm{mg\,mL^{-1}}$). The red bars indicate the height of the isotropic phase. The right inset in the second panel from the bottom shows the position of the X-ray beam (red arrow) through the LLC phase of a two-phase coexistence sample. B) 1D-SAXS profiles for the Poly-T-duplex at various concentrations. C,D) 2D-SAXS patterns for the B-duplex at $184.5\,\mathrm{mg\,mL^{-1}}$ and Poly-T-duplex at $339.4\,\mathrm{mg\,mL^{-1}}$, respectively. Concentration-dependent 1D-SAXS profiles for E) SC-duplex and F) FC-duplex. G,H) 2D-SAXS patterns for the SC-duplex at $300.2\,\mathrm{mg\,mL^{-1}}$ and FC-duplex at $355.1\,\mathrm{mg\,mL^{-1}}$, respectively. The red color in the 2D-SAXS images presented in (C),(D),(G), and (H) corresponds to the highest SAXS intensity. The red dotted line is a guide for the concentration-dependent behavior of q_{DNA} peak. The blue dotted line indicates the concentration coexistence region of a sharp and broad q_{DNA} peak. For each 1D-SAXS profile the corresponding type of phase behavior is also indicated (*I*: isotropic, *N**: chiral nematic or cholesteric, *Sm*-A: smectic A-type and *Col*: columnar). The peak positions relative to fundamental one $q*$ indicate a lamellar structure.

contact of their attractive tips (blunt-ends) resulting to the formation of dimers.

Further information regarding the molecular organization of the SC-duplexes inside the layers can be partially resolved by visual inspection of 2D-SAXS patterns of a partially aligned sample by shear, as shown in Figure 2G. In our case, shear deformation was induced by flow while loading samples into X-ray capillaries. The high-angle reflections associated to correlations along the symmetry axis of SC-duplex (arcs close to the beam stop) are oriented exactly perpendicular to the small-angle reflections which originate from correlations in duplex diameter (the outer broad arc, which corresponds to the q_{DNA} peak in the 1D-SAXS profile). This undoubtedly reveals that the system self-assembled in a *Sm*-A type of mesophase, in which the SC-duplex dimers within the layers are oriented orthogonal to the layer's plane. The narrowed width of the q_{DNA} peak indicates strong positional correlations between the SC-duplex dimers within the smectic layers. This sharp Bragg reflection

ADVANCED
SCIENCE NEWS
www.advancedsciencenews.com

NANO · MICRO
small
www.small-journal.com

could suggest the formation of a smectic-B phase, wherein the dimers are positioned in a hexagonal close-packed array within the layers. However, additional work is required in order to validate this hypothesis. Note that the screening of blunt-end attractions by the 5T-tail for the Poly-T-duplex is not very efficient, since the smectic phase found for the 5T-loop (SC-duplex case) is not found for the Poly-T-duplex, and the same phases are observed as for the B-duplex.

The influence of the full screening of the blunt-end stacking interactions on the LLC phase behavior of the B-duplex is clearly demonstrated by the concentration-dependent 1D-SAXS profiles of the FC-duplex, which are presented in Figure 2F. Similar to the SC-duplex case, a multiple concentration-driven transition sequence from I to $I/N*$ to $N*$ (Figure 2F, second panel from the bottom, $325.4 \, \text{mg mL}^{-1}$ and POM image in Figure S1D, Supporting Information) and finally to a Sm-A type of LLC phase (Figure 2F, third panel from the bottom, $335 \, \text{mg mL}^{-1}$ and aligned 2D-SAXS pattern in Figure 2H). However, the position of the primary peak $q*$ corresponds to a layered structure with a distance between neighboring layers of $d = 2\pi/q* = 18.3 \, \text{nm}$, which is equal to the length of one FC-duplex. This finding undoubtedly supports the molecular packing scenario for the SC-duplexes within the smectic layers and sheds light on the role of this type of weak end-attractive interactions (blunt-ends) in DNA self-assembly. In addition, the layer spacing depends weakly on concentration as revealed by the shift of the Bragg reflections corresponding to the smectic phase toward higher q-values; the first three 1D-SAXS profiles from the top in Figure 2F. This shrinkage in the smectic layer thickness persists at notably high DNA concentrations (a decrease from 18.5 to 16.8 nm on increasing the DNA concentration from 335 to $467.7 \, \text{mg mL}^{-1}$) without any evidence of a *Col* phase. However, we can not exclude the possibility that a *Col* phase might occur at higher DNA densities.

It is worth mentioning that, in both SC- and FC-duplex systems, a SAXS signature of $N*/Sm$-A coexistence similar to the $N*/Col$ transition in B- and Poly-T-duplex systems, is also identified in 1D SAXS profiles of Figure 2E,F (middle panels); a coexistence of a broad and a sharp q_{DNA} peak, with the broad peak's position remaining virtually unchanged through the $N*$ to Sm-A transition (see blue dotted lines).

2.3. Phase Diagrams of B-, Poly-T-, SC-, FC-Duplexes

The phase diagrams as a function of concentration of all-DNA rods with aspect ratio $L/D \approx 8.1$, bending flexibility $L/l_p \approx 0.32$ and different terminal modifications (B-, Poly-T-, SC-, FC-duplex), are presented in **Figure 3** (bottom panel). A combination of SAXS measurements and birefringent textures of the samples as recorded from POM enable us to identify the formed LLC phases. At low DNA concentration, $c < 175 \, \text{mg mL}^{-1}$, all systems are isotropic. Isotropic-to-cholesteric transitions are found to be present in all of the above-mentioned rod-like systems, however, the transitions boundaries are significantly impacted by the type and number of the terminal modifications. The comparison between the phase behavior of the B-duplex and SC-, FC-duplexes clearly shows that the $I/N*$ transition shifts to higher DNA concentrations with decreasing the number of
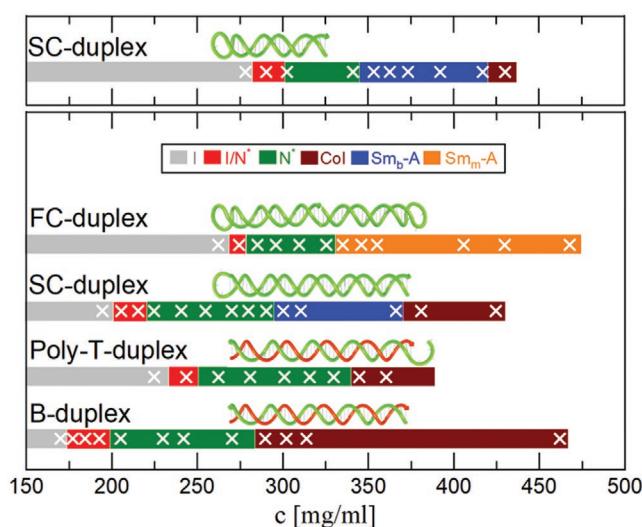

Figure 3. Phase diagram of DNA duplexes with various terminal modifications. Phase diagrams for the B-, Poly-T-, SC-, and FC-duplex with $L_{dsDNA} = 48$ bp in the bottom panel, and for the SC-duplex with $L_{dsDNA} = 24$ bp in the top panel, as a function of the total DNA concentration. The colored regions correspond to different phases (the color code is given in the upper insert of the bottom panel). The white crosses indicate the concentrations that SAXS measurements were performed. Phase identification and determination of the boundaries between the colored regions were carried out by the combination of SAXS experiments, visual inspection of the capillaries between crossed polarizers and polarizing microscopy.

the terminal attractive sites in a rigid blunt-ended DNA duplex (B-duplex). In addition, the above trend is accompanied with a noticeable shrinkage of the $I/N*$ coexistence region (red-marked area in Figure 3, bottom panel). Based on the fact that the strength of the involved terminal base stacking interactions is a few times stronger than the thermal energy[4,31,32] (see also the discussion in the Section 2.4), the above mentioned observations can be understood as a combined effect of both the reduction of the effective molecular elongation and of the length polydispersity in our systems. It is expected that the $I/N*$ phase transition will be postponed to higher DNA concentrations as the effective elongation of the molecule decreases,[13,19,20] while an increase of the system's polydispersity will result to a marked widening of the biphasic region.[12,33–38] Indeed, the partially or fully shielding of the monovalent type of terminal attractions in the B-duplex suppresses significantly the linear aggregation, yielding either to a mixture of dimeric and monomeric species (SC-duplex case) or to pure monomeric species (FC-duplex case).

The influence of molecular elongation in the location of $I/N*$ transition in the SC-duplex system is demonstrated in the top panel of Figure 3, where the concentration-dependent phase diagram of SC-duplex with half-duplex length ($L_{dsDNA} = 24$ bp) is presented (see in Figures S2 and S3, Supporting Information the electrophoresis characterization and representative SAXS profiles, respectively). While this encompasses the same sequence and type of phase transitions, the position of $I/N*$ transition clearly shifts to larger values of the DNA concentration. The results, however, from Poly-T-duplex case, concerning the locations of the phase transitions with respect to the SC-duplex case, are rather surprising. The clear shift of the $I/N*$

ADVANCED
SCIENCE NEWS
www.advancedsciencenews.com

NANO · MICRO
small
www.small-journal.com

transition to higher DNA densities and the narrowing of the corresponding biphasic region compared to B-duplex case suggest that the nonsticky ssDNA dangling tails can definitely disturb the end-to-end stacking interactions, according to previous studies.[4] However, the absence of the smectic phase, combined with the fact that the I/N^* transition takes place at a considerably higher DNA concentrations compared to the SC-duplex, indicates that the Poly-T-duplex system is not a bidisperse mixture of rod-like particles. More detailed structural investigations on the role of length of the dangling tails at the suppression of end-to-end stacking of DNA duplexes with different aspect ratios are probably required to resolve this ambiguity.

The effective inhibition of blunt-end attractions by 5T-loops gives rise to a N^* to Sm-A phase transition, both for the SC- and FC-duplexes. Contrary to the B-duplex, where the N^*/Col phase transition takes place, the stabilization of the smectic phase is a direct consequence of the absence or strongly reduced molecular aggregation by hairpin-mediated capping of the blunt-ends. This is a crucial parameter for accommodating a uniform layer structure, and therefore is energetically favorable the formation of a smectic-A phase with monolayer (Sm_m-A) and bilayer (Sm_b-A) molecular packing for FC-duplex and SC-duplex, respectively. Connected to this, we also find a larger smectic region in the phase diagram, at the expense of the nematic phase for the FC-duplex (bottom panel in Figure 3). Also, an intriguing observation on the phase diagram of Figure 3 is that on further increasing the SC-duplex concentration, a transition from Sm_b-A to Col is obtained, independently of DNA duplex length. In the case of the FC-duplex, however, the Sm_m-A phase is extended to relatively high DNA concentrations without encountering any evidence of a Col phase.

Finally, to probe how an increasing terminal attraction affects the self-assembly behavior of the SC-duplex, without altering the chemical nature of the enthalpic contributions in our system, we exploit the sequence-dependent character of base-pair stacking. The weakest stacking occurs between a AT pair and TA pair (-0.19 Kcal mol^{-1}), and the strongest stacking is at GC/CG (-2.17 Kcal mol^{-1}).[39] As illustrated in Figure 1A, the SC-duplex is blunt-ended with an AT pair. We thus synthesized a SC-duplex terminated with a GC pair. For convenience, we will designate these SC-duplexes as SC-duplex(AT) and SC-duplex(GC), respectively. Similar to the other DNA duplexes employed in this work, the concentration dependence of the self-assembly behavior of the SC-duplex(GC) was investigated using a combination of SAXS and POM experiments The corresponding phase diagram is presented in **Figure 4**, together with the B-duplex and SC-duplex(AT) cases in order to easily demonstrate the influence that blunt-end attraction energy has on the formed LLC states.

Comparison between LLC phase behavior of SC-duplex(AT) and SC-duplex(GC) demonstrates that the sequence of phase transitions from lower to higher DNA concentrations ($I/N^*/Sm_b$-A/Col) remains unchanged by increasing of terminal base stacking attraction. In addition, with an error in DNA concentration measurements of 2%, the critical concentrations at which I/N^* and N^*/Sm_b-A transitions occur are virtually unaffected. We find, however, a noticeable narrowing of the I/N^* coexistence range (see red/green interface, Figure 4) to the benefit of N^* phase. Also, a particularly intriguing observation is
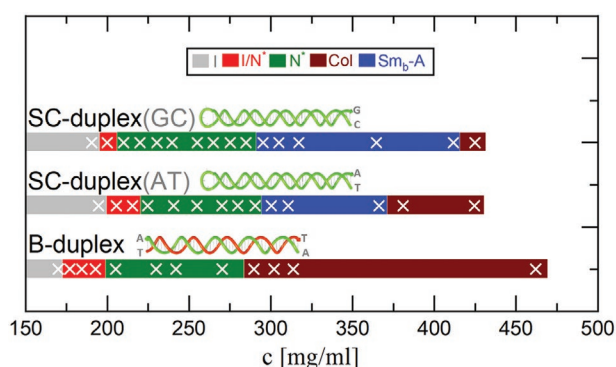

Figure 4. The role of blunt-end attraction strength in the LLC ordering of SC-duplexes. Phase diagrams for SC-duplexes with AT (SC-duplex(AT)) and GC (SC-duplex(GC)) base pair termination as a function of total DNA concentration. The B-duplex and SC-duplex(AT) phase diagrams are re-plotted (see Figure 3, bottom panel) for comparison. All the systems have $L_{dsDNA} = 48$ bp. The color code for the different phases is shown in the upper insert. SAXS measurements were carried out at selected DNA concentrations which are marked by white crosses.

that the Col phase is shrinks in favor of the Sm_b-A phase as the strength of the blunt-end attraction is increased, and therefore, shifting the Sm_b-A/Col transition to higher DNA concentrations (see blue/brown interface, Figure 4).

Up to now we examined the main features of the phase diagrams for FC-duplex and SC-duplex with different end attractions. For a further discussion on their phase behavior, knowledge pertaining to the concentration-dependent fraction of dimers in the SC-duplex system is required. Although the experimental determination of such a quantity is a challenging task, we shall demonstrate in the following section that this information can be extracted from Monte Carlo (MC) simulations. These have been successfully employed in the past to determine the phase behavior of self-assembling monodisperse short linear and gapped DNA duplexes[13,31,40,41] with terminal base stacking free energies similar to the present work. Hence, a further discussion on the reported phase diagrams will be presented in the Section 3 based on a combination of physical arguments extracted from the experimental and simulation results.

2.4. Monte Carlo Simulations

Aiming at obtaining a more rigorous insight into the formation of the emergent LLC mesophases in SC- and FC-duplexes, we perform MC simulations of double and single hairpin-capped duplexes. To account for repulsive interactions, both FC- and SC-duplexes are modeled as hard cylinders (HCs) with length $L = 16$ nm and thickness $D = 2.4$ nm (aspect ratio $X_0 = L/D = 6.67$). Since the SC-duplex exposes an aromatic group on one of its two ends, in this case the modeling HC is also decorated with one interacting site, designated by A. In the inset of **Figure 5**A, site A corresponds to the center of the small red sphere (diameter δ), which is located on the symmetry axis of the cylinder at a distance equal to $L/2 + 0.15D/2$ from the cylinder's center of mass. Sites A of two different cylinders interact *via* a square well (SW) potential $\beta u_{SW} = \beta u_0$ if $r < \delta$ and
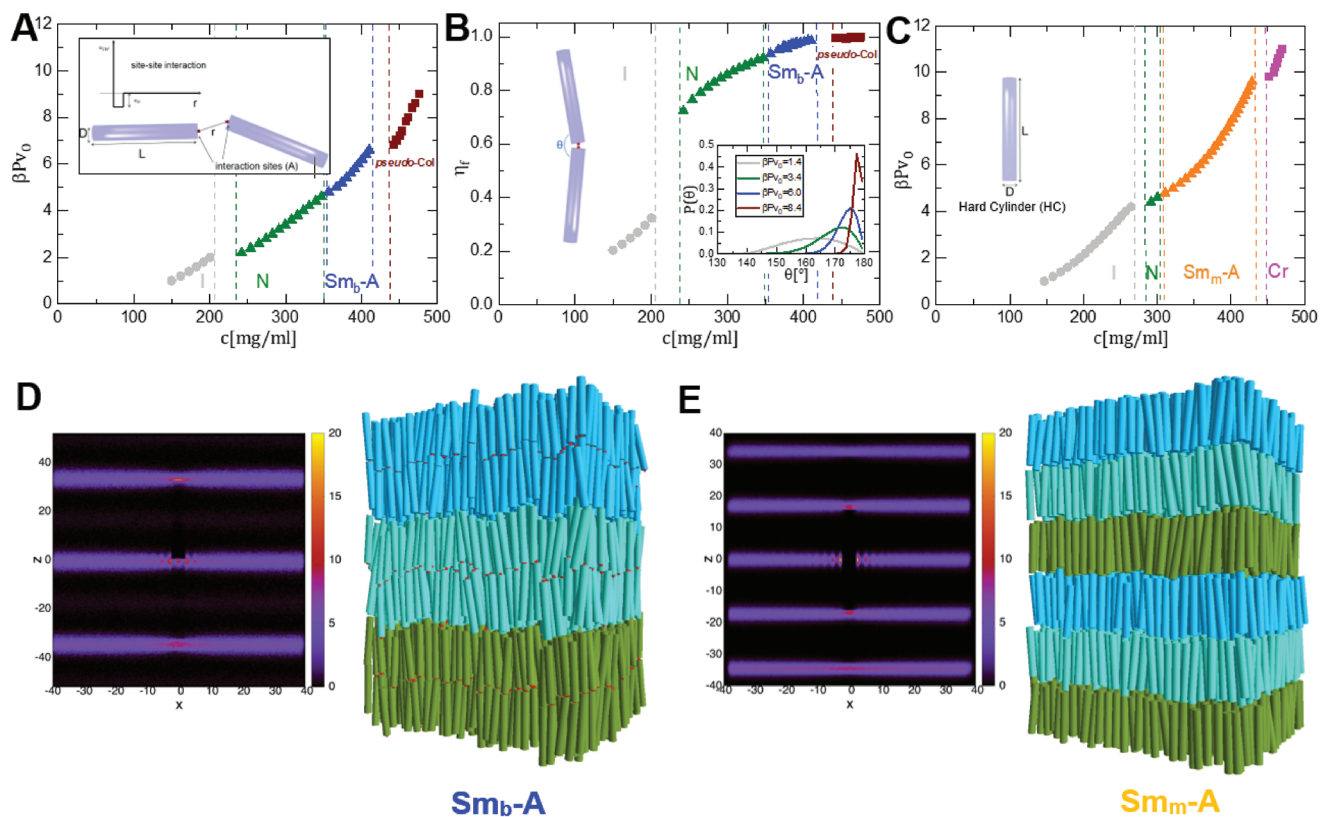
ADVANCED
SCIENCE NEWS
www.advancedsciencenews.com

NANO · MICRO
small
www.small-journal.com

Figure 5. Monte Carlo simulations. A) Equation-of-state for the SC-duplex. Inset: Schematic representation of the model SC-duplexes. The centers of the two small red spheres indicate the sites interacting via the SW potential (shown on the top). The diameter of red spheres represents the interaction range and corresponds to the width of the well. The depth of the well u_0 corresponds to the binding energy. The cylinder diameter is D, and its length is L. B) Fraction of SC-duplex dimers. Inset: Angle dimer distribution, $P(\theta)$, for selected state points: I ($\beta P v_0 = 1.4$), N ($\beta P v_0 = 3.4$), Sm_b-A ($\beta P v_0 = 6.0$), and Col ($\beta P v_0 = 8.4$). C) Equation-of-state for the FC-duplex (modeled as an HC of length L and diameted D) obtained from simulations. D,E) 2D pair-distribution functions $g_\parallel(\mathbf{r}_\parallel)$ and snapshots of selected phases: Sm_b-A, $\beta P v_0 = 6.0$ (D), Sm_m-A, $\beta P v_0 = 9.4$ (E).

$\beta u_{SW} = 0$ if $r > \delta$, where $\delta = (0.5/2.4)D$ is the interaction range which corresponds to the diameter of the sphere centered in site A. The A sites model blunt-end attractions between the terminals of the duplexes,[42] as already proposed in ref. [40]. With an attraction strength between the patches equal to $\beta u_0 = 8.0$, the resulting stacking free-energy corresponds approximately to the one determined previously from the phase behavior[31,40,41] and chiral properties[43] of self-assembling ultra-short DNA duplexes. We take into account the electrostatic repulsion by best matching experimental and numerical phase boundaries through the choice of the diameter $D = 2.4$nm of the HCs, that is, slightly larger than the steric diameter of DNA, which is around 2 nm. In our simulations the FC- and SC-duplex systems consists of $N_L = 6$ particle layers, unless otherwise stated. More details on the simulation can be found in the Experimental Section.

To characterize the phase behavior of the simulated SC- and FC-duplexes, we calculated the equation-of-state (EOS), the fraction of reversibly bonded SC-duplex η_f (SC-duplex dimers), the order parameter, the 3D pair-distribution function $g(\mathbf{r})$,[31] and, we visually inspect configurations (snapshots of selected phases). EOS for SC- and FC-duplexes, which we obtained from simulations, are shown in Figure 5A,C respectively, where the dimensionless pressure $P^* = \beta P v_0$ ($v_0 = $ volume of a single

cylinder) is plotted against the DNA concentration. EOS of SC-duplexes shows a first-order transition from I to a N liquid crystalline state, a second (moving from lower to higher concentrations) transition from the N phase to a Sm-A phase and, finally, a third transition from the Sm-A phase to a columnar phase (pseudo-Col, Figure S4, Supporting Information), which, anyway, is due to finite-size effects as discussed later. The first and last transition are clearly indicated by a discontinuity in the P^* versus concentration curve, while the second transition (N/Sm-A) exhibits a small jump in concentration, suggesting that it is either a weak first order transition or a second order one.

The structure of the Sm-A does appear to exhibit a bilayer morphology (Sm_b-A) as evidenced by the computed 2D pair-distribution function from the patchy unit's center of mass (sites A in Figure 5A) parallel to the nematic director $g_\parallel(\mathbf{r}_\parallel)$ (left panel of Figure 5D) and the snapshot of the corresponding LLC mesophase (right panel of Figure 5D). In the latter, the monovalent attractive patchy units are localized exactly in the middle of the dimer-based smectic layers, which implies that the smectic phase has indeed a bilayer structure.

Concerning the Col phase, in agreement with previous studies,[44,45] it is just caused by finite-size effects if the simulation box size along the nematic axis is not significantly larger

**ADVANCED
SCIENCE NEWS**

www.advancedsciencenews.com

NANO · MICRO

small

www.small-journal.com

than the length of each particle. In particular, starting from the same initial configuration, the columnar phase that is observed in the SC-duplex system with number of particle layers $N_L = 6$ becomes mechanically unstable for $N_L = 16$. The EOS, η_f and angle dimer distributions comparison for these two systems (with $N_L = 6$ and $N_L = 16$) is presented in Figure S5, Supporting Information where in the larger system ($N_L = 16$) a hexagonal crystalline phase Cr is present instead of a Col phase. However, no noticeable system size dependence is observed for the rest of the phase diagram.

A particular intriguing information concerning the molecular conformations within the above-mentioned formed phases can be extracted by computing the degree of SC-duplex dimerization η_f, which is shown in the Figure 5B as a function of concentration. We observe that the I/N transition is accompanied by an abrupt increase of η_f from 0.32 (I) to 0.72 (N), revealing that a significant large portion of the model SC-duplexes exist as dimers already from the nematic phase. The η_f on further increasing the concentration, continuously increases approaching almost the value 1 below the Sm_b-A/pseudo-Col transition; this suggests that the system is exclusively comprised of dimers. In addition, the above mentioned discontinuous jump is followed by a noticeable reduction of the bond angle θ at the junction point of the SC-duplex dimer. Here, θ is the angle between the long axes of the two reversibly bonded SC-duplexes (see schematic of SC-duplex dimer representation in the left inset of Figure 5B). These restrictions are revealed in the computed angular distributions $P(\theta)$ around the I/N transition which are depicted in the right inset of Figure 5B. A distinct width narrowing of $P(\theta)$ and shifting of its maximum toward to larger angle values (dimer straight configuration corresponds to 180°) is observed by increasing the pressure. These tendencies become considerably stronger in the Sm_b-A region (blue curve in the inset of Figure 5B), with the SC-duplex system reaching a full straight configuration of dimers in the pseudo-Col mesophase (brown curve in the inset of Figure 5B).

Concerning the EOS of FC-duplexes shown in Figure 5C, an I/N transition and a second transition to a Sm-A phase are visible. Striking different, however, is the smectic structure compared to the one encountered in the FC-duplex system. This can be clearly seen in the 2D pair-distribution function $g_\parallel(\mathbf{r}_\parallel)$ from the cylinders's center of mass (left panel of Figure 5E) and the snapshot of the corresponding LLC mesophase (right panel of Figure 5F). As expected, similar to the case of monodisperse hard spherocylinders (HSCs),[17,19] the smectic phase has a monolayer morphology (Sm_m-A) with layer thickness comparable to the cylinder's length. Finally, concerning the microscopic ordering of SC- and FC-duplexes within the smectic layers, we extracted equilibrated configurations of hard cylinders from MC simulations and we calculated numerically the total scattering intensity patterns. These theoretical/numerical patterns, as shown in Figure S8, Supporting Information, can be directly compared with their experimental counterparts (Figure 2G,H) and they exhibit the same structural features. The calculation procedure is described in detail in Supporting information (Figure S7, Supporting Information).

Furthermore, we observe a pronounced stabilization of the smectic phase compared to the nematic phase, resulting to a markedly shrinkage of the nematic region, in contrast to the SC-duplex case (see width of N region in Figure 5A). The prevalence of the smectic over the nematic phase in the LLC behavior of our model FC-duplex with aspect ratio $X_0 = 6.67$ is in agreement with results from HSCs (data for $X_0 = 4.0$ in ref. [19]). The wide nematic region appeared in the case of the SC-duplex can be understood in terms of length bidispersity, using a simple packing argument. Since the degree of dimerization η_f varies between the limits 0.72 and 0.92 within the nematic region upon increasing the concentration (Figure 5B), the co-existence of cylinders with two different lengths (monomers and dimers) is expected to interfere with the strict layer thickness requirements pertaining to the smectic order; therefore the N/Sm_b-A transition will be postponed to higher densities. This finding is also supported by MD simulation studies in a binary mixtures of HSCs[46,47] and HCs[48] at the equivalence point, which demonstrate the destabilization of smectic phase on the benefit of the nematic. Eventually, at higher concentrations, both FC- and SC-duplexes (with N_L=16) undergo a transition to a crystal phase (Cr).

Finally, we would like to attract the attention to an earlier MC simulation work on the liquid crystalline phase behavior of dimerizing HSCs.[49] The authors employed HSCs with an attractive square well of depth $\beta u_0 = 7.0$ at one end, and aspect ratio of $L/D = 5$. These parameters are quite similar to those used for modeling the SC-duplexes. Interestingly, no evidence for the existence of Sm_b-A is found. Instead, this study revealed the formation of a Sm_m-A phase, and, essentially coincides with the phase behavior of purely repulsive HSCs system. The discrepancies between the MC studies of ref. [49] and of our work suggest that the stabilization of the Sm_b-A, mediated by the presence of single attractive sites on the tips of the HSCs, may strongly depend on the geometry of these attractive patches. We can speculate that the lack of Sm_b-A in the latter study can be likely ascribed to the high flexibility of dimer bonds due to the large volume available for bonding of the patches. However, further studies are necessary for verifying this speculation.

3. Discussion

The MC simulations, employing the above discussed coarse-grained molecular models, confirm the stability of the experimentally found LLC phases, with the notable exception the Col phase, demonstrating a fair quantitative agreement with experiments on the location of I/LLC transition. In addition, the simulations are able to capture qualitatively the majority of the experimentally reported changes in the LLC phase behavior arising from the interplay between the interaction energy and the directionality of interactions. Concerning the occurrence of Col phase, experiments show that the phase behavior of the FC-duplex differs markedly from the behavior of the SC-duplex. In the case of the FC-duplex, we did not encounter any evidence for Sm_m-A/Col transition over the investigated concentration range, in contrast to the SC-duplex where the presence of the single blunt-end attraction seems to stabilize the Col mesophase. Finally, for the case of the SC-duplex, the experiments reveal that increasing the strength of terminal attraction diminishes the range of stability of the Col phase. The region

of the Sm_b-A phase widens, shifting of the Col phase into the direction of higher DNA concentrations (see blue/brown interface in Figure 4). This result is not unexpected, since stronger binding energies between experimental SC-duplexes can result to an increase of dimer stiffness.

Understanding the emergence of Col phase in SC-duplexes and how the attraction strength between their monovalent patches becomes significant near the LLC transitions require to consider the balance of many factors including effective molecular elongation, length polydispersity and flexibility. Our simulations predict that the degree of dimerization reaches a value of $\eta_f \approx 1.0$ at the Sm_b-A/pseudo-Col transition (Figure 5B). This implies that the SC-duplexes can be viewed as simply FC-duplexes with double length. However, the possibility that the aspect ratio enhancement upon dimerization may lead to the formation of Col has to be ruled out, since a Sm_b-A/Col transition is also observed in the experimental phase diagram of SC-duplex with half duplex length (top panel of Figure 3).

So far, it is well understood that the Col phase can be stabilized by length polydispersity in a system of hard rods. This effect has been assessed by several theoretical, experimental and computer simulation studies, involving systems with a continuous distribution of molecular length[48,50] or finite-size dispersity.[46,47,51] In particular, concerning DNA-based LLCs, the above types of length polydispersity are pertaining either to their inherent molecular property[9] or to the presence of monovalent terminal attractive interactions.[4,13,31,52] However, according to the present model employed for simulating the SC-duplexes, a stabilization mechanism of Col phase originated from bidispersity is a rather implausible scenario since the SC-duplexes are completely dimerized as indicated from the values of η_f in the proximity of Sm_b-A/pseudo-Col transition (Figure 5B). The latter implies the SC-duplexes with half duplex length (L_{dsDNA} = 24 bp) has effectively the same molecular length with the FC-duplexes (L_{dsDNA} = 48 bp) at DNA concentrations where the SC-duplexes undergo a transition from smectic to columnar phase (Figure 3, top panel). In addition, the dimerization mechanism effectively blocks the attractive terminal sites, and, therefore these two systems in terms of aspect ratio and interactions are indistinguishable. Hence, the most obvious difference is the bending flexibility at the junction point of the SC-duplex dimers. It is, however, imperative to note that terminal base pairs in DNA duplexes in solutions are known to exhibit a frequent and reversible opening via so-called "fraying" mechanism.[53–55] These transient opening events may weaken the stacking attraction between the blunt-ended DNA duplexes and in turn it can be viewed as an effective reduction of the number of SC-duplexes able to dimerize, thus introducing a concentration independent amount of length polydispersity in the system. A simulation model that can capture the "fraying" mechanism could provide an insight into the importance of this phenomenon in the SC-duplex phase behavior.

In the phase diagram of SC-duplexes presented in Figure 3, it is expected that the impact of internal flexibility at their association point (dimer's junction) will be most noticeable when the degree of dimerization η_f becomes significantly large, and, hence, there is no interference from the bidispersity effect. Our simulations indicate that this is the case for DNA concentrations around the N/Sm_b-A transition, with η_f reaching values above 0.9 (Figure 5B). Indeed, the phase behavior comparison between the FC-duplexes (Figure 3, bottom panel) and the SC-duplexes (Figure 3, top panel), which in dimer form have equal effective molecular length with FC-duplexes, demonstrate that flexibility raises the DNA concentration at the $N*/Sm_b$-A transition, in agreement with theoretical[56,57] and simulation.[58–60] predictions. Also we observe that the $I/N*$ phase transition concentration is shifted toward larger values, accompanied by a small but a noticeable shrinkage of the $N*$ region. These results are in accordance with the predictions of refs. [56, 61–65] as well as the computer simulation studies[58,60,66] on the influence of flexibility in this type of LLC phase and transition. However, our simulations indicate that near the $I/N*$ phase transition the degree of dimerization η_f is strongly concentration dependent (varied between 0.3 and 0.8 in Figure 5B), and, therefore, it will be quite premature to attribute the above phase behavior solely to flexibility since in this concentration region the effects of bidispersity and flexibility are strongly intertwined. This is also supported from the observed widening of the $I/N*$ biphasic region in the SC-duplex, which follows the opposite to predictions trend.

The role of flexibility in the phase diagram SC-duplex system is additionally demonstrated in Figure 4. It is expected that the flexibility at the dimer's junction point will be decreased by increasing the blunt-end attraction strength, as already discussed. The increase of attraction strength between the terminal sites of the SC-duplexes strongly affects the Sm_b-A/Col transition by raising its concentration (blue/brown interface in Figure 4), without, however, affecting significantly the location of $N*/Sm_b$-A transition (green/blue interface in Figure 4). For the SC-duplex(GC) case, the narrowing of the $I/N*$ biphasic region in favor of the $N*$ phase is most probably due to the increase of the degree of dimerization η_f due to the enhanced base stacking interactions compared to the SC-duplex(AT) case. We also note that the degree of dimerization can be further enhanced by "fraying" effect, which is expected to be weaker in SC-duplexes(GC) than in SC-duplexes(AT).[54]

To investigate in a more detail fashion the effect of base stacking energies between the blunt-ends of SC-duplexes we carried out simulations for attraction strengths between 6.7 k_BT (weak limit) and 11.9 k_BT (strong limit). The geometry and interaction potential of the A sites in the model SC-duplexes at hand do not allow to capture the flexibility effect at their association point. Nevertheless, the attraction strength dependence of the EOS and dimer's fraction η_f as a function of concentration are particular interesting, and, they are demonstrated in Figure S6, Supporting Information. It can be seen that increasing the attraction strength the abrupt change in the degree of dimerization at the I/N transition is diminished. For strong end-attractions (>8.0 k_BT), the η_f reaches values above 0.8 for concentrations just above the I/N biphasic region. The same phase sequence at all attractions is observed, with the location of Sm_b-A/pseudo-Col transition to be independent of the attraction strength. The latter is not surprising since our model SC-duplexes at the proximity of this LLC transition have a high degree of dimerization, being $\eta_f > 0.97$ for the explored stacking energies, i.e we are almost in the regime of full dimerization for all attraction strengths studied, and in

our model the flexibility of the bonds is independent of the attraction strength.

In addition, the results of Figure S6, Supporting Information reveal that the increase of the attraction strength shifts weakly the location of the N/Sm_b-A at lower concentrations with a slight widening of the corresponding biphasic region (see shadow regions). The same trend also holds for the location of I/N transition, however, it is accompanied with a noticeable narrowing of the corresponding biphasic region. The above simulation findings on the effects of end-attraction strength in the LLC phase behavior of the SC-duplex system, excluding the case of Sm_b-A/pseudo-Col transition, qualitatively agree with experiments (Figure 4).

It is worth mentioning that molecular dynamics simulations of model rod-like particles with similar values of aspect ratio and flexibility to our experimental SC-duplex system, which are decorated with a single weak attractive tip modeled by a Lennard–Jones potential, predict the existence of a Sm_b-A phase without any evidence of a stable Col phase.[67] However, a recent experimental study on the LLC behavior of aqueous solutions of monodisperse rod-like filamentous viruses[68] having one tip functionalized with hydrophobic fluorescent dyes, and with a similar flexibility as considered in ref. [67], but one order of magnitude higher aspect ratio, did not reveal the formation of an equilibrium Sm_b-A phase. We attribute the lack of a clear evidence of an experimental bilayer smectic phase to the multivalent character of this type of terminal modification which most probable allows branching at the viruses' association points. Our results, therefore, suggests that at least from an experimental point of view, the key element for the existence of thermodynamic stable Sm_b-A phase is the monovalent attractive character of the blunt-end stacking interactions which give rise to a stiff enough bond.

4. Conclusion

The role of the weak blunt-end base stacking interactions in all-DNA LLC self-assembly is investigated by both experiments and simulations. Phase diagrams were determined over a wide concentration range for stiff DNA duplexes which differ in their terminal attractive interactions. Control over these intermolecular stacking forces was achieved either by selectively capping the DNA duplex's terminal sites (SC- and FC-duplexes, Figure 1A) or by altering the type of the terminal base-pair (SC-duplex blunt-ended with AT or GC pair, first two cartoons from the top in Figure 4). Our results unequivocally demonstrate that thermodynamically stable bilayer (Sm_b-A) and monolayer (Sm_m-A) smectic A-type of LLC phases in concentrated aqueous-saline solutions of rigid dsDNA fragments can be stabilized by completely suppressing the attraction in the one (SC-duplex) or both (FC-duplex) tips of the DNA helices, respectively. These findings offer a conclusive evidence that weak monovalent stacking attraction mediated by the presence of blunt-ends in the DNA helices is the reason for the lack of smectic phase in concentrated solutions of stiff dsDNA fragments with sufficient shape anisotropy.

Overall, we demonstrated that non-covalent DNA base-stacking interactions allow to engineer well-defined monovalent

attractive patches. DNA bases stack weakly to moderately, however, due to rapid developments in the fields of synthetic chemistry and automated synthesis of oligonucleotides, is feasible to integrate a variety of non-natural bases that attract each other by stacking interactions more strongly than the natural ones.[1] This points the way toward the creation of a palette of patches with tunable attraction strength, which in combination with carefully ssDNA sequence design, can easily allow their user-prescribed positioning on the surface of an all-DNA rigid structure with sub-nanometer precision (at single base level). In addition, given the great advances in the field of structural DNA nanotechnology on the fabrication of highly anisotropic, stiff and complex in shape all-DNA nanostructures,[69] we anticipate, that high levels of assembly information can be encoded to all-DNA liquid crystalline building blocks by controlling the directionality of their interactions through engineered shape anisotropy and patchiness. This eventually may lead to the realization of novel programmable LLC self-assembly pathways and the formation of intriguing LLC phases such as the reported all-DNA Sm_b-A phase. Finally, our work in the role of blunt-ends in DNA LLC behavior could prove useful beyond the static DNA self-assembly. These weak stacking interactions with controllable strength could allow an externally triggered dynamic assembly and disassembly of filament-like all-DNA liquid crystal elastomer structures that may mimic key aspects of the functional sophistication of the cell's cytoskeleton. Furthermore, expanding the above-mentioned concept to realize dynamic 3D all-DNA structures could pave the way for development of a new promising class of materials for specific therapeutic (drug-delivery vehicles) and diagnostic (biosensing platform nanotechnologies) applications.

5. Experimental Section

Synthesis and Characterization of Capped DNA Duplexes: All DNA strands were purchased from Biomers and purified by HPLC. Oligonucleotide sequences are shown in Figure 1A. The DNA duplexes were formed using a standard annealing protocol reported previously,[13] and the products were analyzed under nondenaturing PAGE. Samples were prepared by step-like dilution with 1xTE/Na buffer solution (10 mm Tris, pH 8.0, 150 mm NaCl) from highly concentrated solutions.[13] The corresponding ionic strength was 160.0 mm. A microvolume spectrometer (NanoDrop 2000) was used for measuring the DNA concentration.

SAXS: SAXS experiments were carried out at the high brilliance Galium Anode Low Angle X-ray Instrument (GALAXI) of the Jülich Center for Neutron Science (JCNS, Germany).[70] The samples were measured at a sample-to-detector distance of 1.706 m with a flux of 10^9 photons s^{-1} mm^{-2} at 0.3 mrad divergence of the beam at sample position. A Dectris–Pilatus 1M detector with resolution of 981 × 1043 pixels and a pixel size of 172 × 172 µm^2 was employed to record the 2D SAXS scattering patterns. The 2D SAXS patterns were integrated using FIT2D software. The DNA solution was thoroughly homogenized (up to 3 days for the more viscous samples) ensuring the absence of spatial concentrations gradients before loading into capillaries (2 mm thickness borosilicate, Hilgenberg) for SAXS experiments.[13]

MC Simulations: NPT MC simulation of N = 3360 SC- and FC-duplexes modeled as hard cylinders with and without an interacting site were performed as discussed in the section on MC simulations. The three directions of the box were allowed to change independently in the MC simulations to ease the formation of mesophases and periodic boundary conditions were used. All the results from simulations

ADVANCED
SCIENCE NEWS
www.advancedsciencenews.com

NANO · MICRO
small
www.small-journal.com

(i.e., pair-distribution function, concentration, energy, etc.) were obtained by performing 10^8 MC steps and by discarding the initial equilibration stage. Such huge number of steps were made possible by employing a recently developed algorithm for simulating hard cylinders[71] which relied on a novel and very efficient algorithm for finding the roots of a quartic equation.[72] The initial configuration used for the equilibration was obtained by placing the hard cylinders on a ortorhombic lattice.[19,73] To check that the columnar phase observed for SC-duplexes was only due to finite-size effects, simulations of larger systems composed of $N = 7744$ HC were also performed. More details can be found in the Figure S4, Supporting Information.

Supporting Information

Supporting Information is available from the Wiley Online Library or from the author.

Acknowledgements

Conflict of Interest

The authors declare no conflict of interest.

Author Contributions

K.G. and S.N.R. contributed equally to this work. E.S. conceived the project and designed research; K.G., S.N.R., and E.S. synthesized the all-DNA nanostructures and performed experiments; E.K. and U.R. operated the SAXS beamline; A.G.O. and C.D.M. performed the Monte Carlo simulations; J.K.G.D. contributed to initiating the project and data interpretation; E.S. wrote the manuscript with support from C.D.M. All co-authors commented on the manuscript.

Data Availability Statement

The data that support the findings of this study are available from the corresponding author upon reasonable request.

Keywords

[1] K. M. Guckian, B. A. Schweitzer, R. X.-F. Ren, C. J. Sheils, D. C. Tahmassebi, E. T. Kool, *J. Am. Chem. Soc.* **2000**, *122*, 2213.
[2] J. D. Watson, F. H. Crick, *Nature* **1953**, *171*, 737.
[3] E. T. Kool, *Annu. Rev. Biophys. Biomol. Struct.* **2001**, *30*, 1.
[4] M. Nakata, G. Zanchetta, B. D. Chapman, C. D. Jones, J. O. Cros, R. Pindak, T. Bellini, N. A. Clark, *Science* **2007**, *318*, 1276.
[5] G. Zanchetta, T. Bellini, M. Nakata, N. A. Clark, *J. Am. Chem. Soc.* **2008**, *130*, 12864.
[6] S. Woo, P. W. K. Rothemund, *Nat. Chem.* **2011**, *3*, 620.
[7] T. Gerling, K. F. Wagenbauer, A. M. Neuner, H. Dietz, *Science* **2015**, *347*, 1446.
[8] T. E. Strzelecka, M. W. Davidson, R. L. Rill, *Nature* **1988**, *331*, 457.
[9] F. Livolant, A. M. Levelut, J. Doucet, J. P. Benoit, *Nature* **1989**, *339*, 724.
[10] H. H. Strey, J. Wang, R. Podgornik, A. Rupprecht, L. Yu, V. A. Parsegian, E. B. Sirota, *Phys. Rev. Lett.* **2000**, *84*, 3105.
[11] F. Livolant, A. Leforestier, *Prog. Polym. Sci.* **1996**, *21*, 1115.
[12] K. Merchant, R. L. Rill, *Biophys. J.* **1997**, *73*, 3154.
[13] M. Salamonczyk, J. Zhang, G. Portale, C. Zhu, E. Kentzinger, J. T. Gleeson, A. Jakli, C. D. Michele, J. K. G. Dhont, S. Sprunt, E. Stiakakis, *Nat. Commun.* **2016**, *7*, 13358.
[14] M. Siavashpouri, C. H. Wachauf, M. J. Zakhary, F. Praetorius, H. Dietz, Z. Dogic, *Nat. Mater* **2017**, *16*, 849.
[15] L. Onsager, *Ann. N.Y. Acad. Sci.* **1949**, *51*, 627.
[16] M. Franco-Melgar, A. J. Haslam, G. Jackson, *Mol. Phys.* **2008**, *106*, 649.
[17] D. Frenkel, *J. Phys. Chem.* **1987**, *91*, 4912.
[18] D. Frenkel, H. N. W. Lekkerkerker, A. Stroobants, *Nature* **1988**, *332*, 882.
[19] S. C. McGrother, D. C. Williamson, G. Jackson, *J. Chem. Phys.* **1996**, *104*, 6765.
[20] P. Bolhuis, D. Frenkel, *J. Chem. Phys.* **1997**, *106*, 666.
[21] P. Gyawali, R. Saha, G. P. Smith, M. Salamonczyk, P. Kharel, S. Basu, R. Li, M. Fukuto, J. T. Gleeson, N. A. Clark, A. Jákli, H. Balci, S. Sprunt, *Proc. Natl. Acad. Sci. USA* **2021**, *118*, e2019996118.
[22] Z. Dogic, S. Fraden, *Phys. Rev. Lett.* **1997**, *78*, 2417.
[23] E. Grelet, *Phys. Rev. X* **2014**, *113*, 268303.
[24] A. Kuijk, D. V. Byelov, A. V. Petukhov, A. van Blaaderen, A. Imhof, *Faraday Discuss.* **2012**, *159*, 181.
[25] L. Li, S. A. Pabit, J. S. Lamb, H. Y. Park, L. Pollack, *Appl. Phys. Lett.* **2008**, *92*, 223901.
[26] R. Wang, A. Kuzuya, W. Liua, N. C. Seeman, *Chem. Commun.* **2010**, *46*, 4905.
[27] C. Ke, M. Humeniuk, H. S-Gracz, P. E. Marszalek, *Phys. Rev. Lett.* **2007**, *99*, 018302.
[28] C. A. G. Haasnoot, J. H. J. den Hartog, J. F. M. de Rooij, J. H. van Boom, C. Altona, *Nucleic Acid Res.* **1980**, *8*, 169.
[29] C. A. G. Haasnoot, S. H. de Bruin, R. G. Berendsen, H. G. J. M. Janssen, T. J. J. Binnendijk, C. W. Hilbers, *J. Biomolec. Struct. Dyn.* **1983**, *1*, 115.
[30] D. Durand, J. Doucet, F. Livolant, *J. Phys. II* **1992**, *2*, 1769.
[31] C. De Michele, T. Bellini, F. Sciortino, *Macromolecules* **2012**, *45*, 1090.
[32] F. Kilchherr, C. Wachauf, B. Pelz, M. Rief, M. Zacharias, H. Dietz, *Science* **2016**, *353*, aaf5508.
[33] S. Fraden, G. Maret, D. L. D. Caspar, *Phys. Rev. E* **1993**, *48*, 2816.
[34] H. N. W. Lekkerkerker, P. Coulon, R. V. D. Haegen, R. Deblieck, *J. Chem. Phys.* **1984**, *80*, 3427.
[35] T. M. Birshtein, B. I. Kolegov, V. A. Pryamitsyn, *Polym. Sci. USSR* **1988**, *30*, 316.
[36] G. Vroege, H. N. W. Lekkerkerker, *Rep. Prog. Phys.* **1992**, *55*, 1241.
[37] Z. Y. Chen, *Phys. Rev. E* **1994**, *50*, 2849.
[38] H. H. Wensink, G. J. Vroege, *J. Chem. Phys.* **2003**, *119*, 6868.
[39] E. Protozanova, P. Yakovchuk, M. D. Frank-Kamenetskii, *J. Mol. Biol.* **2004**, *342*, 775.
[40] K. T. Nguyen, F. Sciortino, C. De Michele, *Langmuir* **2014**, *30*, 4814.
[41] C. De Michele, L. Rovigatti, T. Bellini, F. Sciortino, *Soft Matter* **2012**, *8*, 8388.

[42] L. Rovigatti, F. Bomboi, F. Sciortino, *J. Chem. Phys.* **2014**, *140*, 154903.

[43] C. De Michele, G. Zanchetta, T. Bellini, E. Frezza, A. Ferrarini, *ACS Macro Lett.* **2016**, *5*, 208.

[44] J. A. C. Veerman, D. Frenkel, *Phys. Rev. A* **1991**, *43*, 4334.

[45] S. Dussi, M. Chiappini, M. Dijkstra, *Mol. Phys.* **2018**, *116*, 2792.

[46] A. Stroobants, *Phys. Rev. Lett.* **1992**, *69*, 2388.

[47] A. Stroobants, *J. Phys.: Condens. Matter* **1994**, *6*, A285.

[48] A. M. Bohle, R. Holyst, T. Vilgis, *Phys. Rev. Lett.* **1996**, *76*, 1396.

[49] S. C. McGrother, R. P. Sear, G. Jackson, *J. Chem. Phys.* **1997**, *106*, 7315.

[50] M. A. Bates, D. Frenkel, *J. Phys. Chem.* **1998**, *109*, 6193.

[51] S. Varga, E. Velascob, L. Mederos, F. J. Vesely, *Mol. Phys.* **2009**, *107*, 2481.

[52] T. Kuriabova, M. D. Betterton, M. A. Glaser, *J. Mater. Chem.* **2010**, *20*, 10366.

[53] D. Andreatta, S. Sen, J. L. Pérez Lustres, S. A. Kovalenko, N. P. Ernsting, C. J. Murphy, R. S. Coleman, M. A. Berg, *J. Am. Chem. Soc.* **2006**, *128*, 6885.

[54] M. Zgarbová, M. Otyepka, J. Šponer, F. Lankaš, P. Jurečka, *J. Chem. Theory Comput* **2014**, *10*, 3177.

[55] P. J. Sanstead, P. Stevenson, A. Tokmakoff, *J. Am. Chem. Soc.* **2016**, *138*, 11792.

[56] P. van der Schoot, *J. Phys. II France* **1996**, *6*, 1557.

[57] A. V. Tkachenko, *Phys. Rev. E* **1998**, *58*, 5997.

[58] P. Bladon, D. Frenkel, *J. Phys.: Condens. Matter* **1996**, *8*, 9445.

[59] G. Cinacchi, L. D. Gaetani, *Phys. Rev. E* **2008**, *77*, 051705(4).

[60] B. de Braaf, M. O. Menegon, S. Paquay, P. van der Schoot, *J. Chem. Phys.* **2017**, *147*, 244901.

[61] A. R. Khokhlov, A. N. Semenov, *Phys. A* **1981**, *108*, 546.

[62] A. R. Khokhlov, A. N. Semenov, *Phys. A* **1982**, *112*, 605.

[63] T. Odijk, *Macromolecules* **1986**, *19*, 2313.

[64] A. V. Tkachenko, *Phys. Rev. Lett.* **1996**, *77*, 4218.

[65] Z. Y. Chen, *Macromolecules* **1993**, *26*, 3419.

[66] M. Dijkstra, D. Frenkel, *Phys. Rev. E* **1995**, *51*, 5891.

[67] M. O. Menegon, G. L. A. Kusters, P. van der Schoot, *Phys. Rev. E* **2019**, *100*, 042702.

[68] A. Repula, M. O. Menegon, C. Wu, P. van der Schoot, E. Grelet, *Phys. Rev. Lett.* **2019**, *122*, 128008.

[69] N. C. Seeman, H. F. Sleiman, *Nat. Rev. Mater.* **2017**, *3*, 17068.

[70] Jülich Centre for Neutron Science, *J. Large-Scale Res. Facil.* **2016**, *2*, A61.

[71] A. G. Orellana, E. Romani, C. De Michele, *Eur. Phys. J. E* **2018**, *41*, 51.

[72] A. G. Orellana, C. D. Michele, *ACM Trans. Math. Softw.* **2020**, *46*, 20.

[73] D. Frenkel, *J. Phys. Chem.* **1988**, *92*, 3280.